

Feynman-Enderlein Path Integral for Single-Molecule Nanofluidics

Siddharth Ghosh^{†*}

Department of Applied Mathematics and Theoretical Physics, University of Cambridge, Cambridge, UK.

Yusuf Hamied Department of Chemistry, University of Cambridge, Cambridge, UK.

Maxwell Centre, Cavendish Laboratory, University of Cambridge, Cambridge, UK.

St John's College, University of Cambridge, Cambridge, UK.

I present a photon statistics method for quasi-one dimensional sub-diffraction limited nanofluidic motions of single molecules using Feynman-Enderlein path integral approach. The theory is validated in Monte Carlo simulation platform to provide fundamental understandings of Knudsen type flow and diffusion of single molecule fluorescence in liquid. Distribution of single molecule burst size can be precise enough to detect molecular interaction. Realisation of this theoretical prediction considers several aspects of single-molecule nanofluidics, such as electrodynamics, photophysics, and multi-molecular events/molecular shot noise. I study two different sizes of molecules, one with 2 nm and another 20 nm hydrodynamic radii and found two distinctly different nanofluidic regimes, which have not been theoretically as well as experimentally reported earlier. The method is not restricted to single molecule environment of uniform electrodynamic interactions. It can be used to understand complex refractive index mismatch related non-uniform single-molecule electrodynamic interactions as well. The method uses experimental data of single-molecule fluorescence inside nanofluidic channels. This work has a potential to accelerate the progress of complex single-molecule experiments, such as dynamic heterogeneity, biomolecular interactions of misfolded proteins, and nanometric cavity electrodynamics.

I. INTRODUCTION

In dynamic single-molecule experiments [1–4], for example in single molecule nanofluidics [5, 6], one of the hardest problems is to identify if the signals are purely single-molecule events due to the convoluted complexity associated with electrodynamic interactions/Purcell effect [7–10], photophysics [11, 12], electrostatic effect [13, 14], multi-molecular interactions [15], and confined/Knudsen diffusion [16, 17]. Feynman described this problem as, “...as we go down in size, there are a number of interesting problems that arise. All things do not simply scale down in proportion... There will be several problems of this nature that we will have to be ready to design for.” [18]. Statistical mechanics at nanometric length scale and molecular self assembly can potentially answer many questions related to life on earth as well as reveal unfamiliar physics [19–25]. Tracking of single molecules [26] has been a centre of this field [2, 27] where increasing accuracy of spatial position and temporal information for dynamic behaviour of a molecule in two dimensions were two key problems. The state-of-the-art solid-state and soft nanoengineering provides sufficient precision to handle individual single molecules by overcoming diffusion induced slip from detection volume and non-uniform electrodynamics induced artefacts in single-molecule fluorescence signals. In this paper, by nanofluidic, I am referring to Knudsen flow/diffusion environment where two spatial dimensions are close to or smaller

than the mean free path of molecule’s diffusion as well as smaller spatial confinement than the wavelength of light being used for single-molecule detection [6]. Examples of such environment are molecular motion inside tunnelling nanotube or membrane nanotube [28], nanopores, single molecule sequencing - linearise DNA in nanochannel array [29], zeolite-catalysis [30], and mass transfer in carbon nanotubes [31, 32]. Diffraction limited detection of these single-molecule nanofluidic motions possess two problems – (a) how do we know that a single molecule is flowing or crawling in the detection volume? (b) How do we know that more than one molecule are present in the detection volume? Photon antibunching [33] and stepwise photobleaching [34] are two widely used methods to resolve this spatio-temporal problem. Those two strategies are not useful for dynamic systems since photon statistics is limited by the number of photons. Single-molecule methods have gained a significant popularity to becoming a standard in analytical chemistry and structural biology as predicted by Keller [35]. However, the limited understanding of this spatio-temporal problem is restricting single-molecule spectroscopy at its fullest advantage within the mathematical physics and physical-chemistry communities. Single-molecule spectroscopists should have the ability to model the transient behaviour of the molecules through a confocal laser beam considering the molecule cycles through excitation and emission, which produces photon emission and significantly influenced by the aforementioned parameters.

I demonstrate a method to overcome this barrier and to predict and model the characteristics of single-molecule bursts and their spatio-temporal distributions inside nanofluidic environment. The transiting single molecules through the focus do not have enough time to provide the reasonable number of photons to perform

* sg915@cam.ac.uk; also affiliated to Single-Molecule Optics Group, Huygens Laboratory, Leiden Institute of Physics, Leiden University, The Netherlands. Open Academic Research UK CIC, Cambridge, UK. Open Academic Research Council, Hyderabad, India.

the antibunching or photobleaching. In contrast, burst size distribution [15] or burst variant analysis with dynamic heterogeneity and static heterogeneity [11, 36] provides useful information to distinguish between molecular shot noise [37], multi-molecule events, and single-molecule events.

The Feynman-Enderlein path integral approach in Monte Carlo (FEPI MC) is presented for two different sizes of single molecules – 2 nm and 20 nm. I have performed the simulation for two overlapping cofocal foci as used in two-foci correlation spectroscopy [38, 39]. The advantage of having two foci over a single focus is that it can extract the velocity of the flowing molecules, which is difficult to obtain in a single focus setup where the method depends strongly on the complex molecular detection function [40, 41]. If we can solve the problem for a two foci system, information for transiting molecules through a single focus can be extracted by turning off another focus in the simulation.

II. COMPUTING BURST SIZE DISTRIBUTION

I use the Feynman path integral [42] to model single molecule burst size distribution using the burst searching theory developed by Enderlein et al. [15, 43]. Hence, I term the modified path integral for single-molecule fluorescence as Feynman-Enderlein path integral. I look into the temporal probability of existence of an unbleached single molecule while passing through a confocal laser beam. The existence probability decay exponentially after detecting a photon when no further photon is detected. Once the next photon gets detected instantaneously the probability goes to a larger value due to a possibility of a photon being emitted from the molecule

instead of the background. The non-vanishing probability of background photon keeps the existence probability always less than unity. This time evolution of the existence probability is an important model for single molecule burst identification. It is unavoidable to ignore the photobleaching effect from the expression of the existence probability within a given time interval in case of single-molecule nanofluidics. Derivation for the photobleaching contribution can be found in [43].

For pure single-molecule transits, let us consider that at $\tau = 0$ when the molecule with trajectory $\mathbf{r}(\tau)$ started flowing outside the confocal volume, and $\tau = T$ is large enough to consider that the molecule have crossed the detection volume. The existence probability of single molecule BSD is given by $P_1(N)$ where 1 stands for ‘single-molecule crossing’. In the model, I have considered one-step photobleaching and negligible triplet-state (longer triplet state can be handled as well). A simple Poisson distribution can describe the photon detection statistics of these single molecules’ sub-subensemble as

$$X_f = \int_0^\tau X_f[\mathbf{r}(\tau)]d\tau \quad (1)$$

where within the time interval $\delta\tau$ the molecule at position \mathbf{r} gives rise to the probability of detecting a photon as $X_f(\mathbf{r})\delta\tau$. The probability of detecting N photons during the time interval $\{0, T\}$ will be superposition of these Poisson distributions as (equation 2),

$$P_1(N) = \int_0^\infty \frac{X_f^N}{N!} \exp(-X_f) \cdot P[X_f]dX_f \quad (2)$$

where $P[X_f]$ is the distribution function in a form of a path integral, which runs over all possible photobleaching times and molecular trajectories.

$$P[X_f] = \int_0^T \int D\mathbf{r}(\tau) \delta \left[X_f - \int_0^{\tau_{bl}} X_f[\mathbf{r}(\tau)] \right] X_{bl}[\mathbf{r}(\tau_{bl})] d\tau_{bl} \times \exp \left[- \int_0^{\tau_{bl}} \left(\frac{[\mathbf{r}(\tau) - \mathbf{v}]^2}{4D} + X_{bl}[\mathbf{r}(\tau)] \right) d\tau \right] p_0[\mathbf{r}_0] + \int D\mathbf{r}(\tau) \delta \left[X_f - \int_0^T X_f[\mathbf{r}(\tau)] d\tau \right] \times \exp \left[- \int_0^T \left(\frac{[\mathbf{r}(\tau) - \mathbf{v}]^2}{4D} + X_{bl}[\mathbf{r}(\tau)] \right) d\tau \right] p_0[\mathbf{r}_0] \quad (3)$$

The $\delta[f(\mathbf{r})]$ is δ -function functional, $p_0(\mathbf{r}_0)\delta\mathbf{r}$ is the probability of finding a molecule in the small volume $\delta\mathbf{r}$ at position \mathbf{r}_0 at time $t = 0$, $\delta\tau X_{bl}\mathbf{r}$ is the probability of photobleaching the molecule within $\delta\tau$ at position \mathbf{r} , D is the diffusion constant of the molecule, and \mathbf{v} is the flow velocity. The path integration $\int D\mathbf{r}(\tau)$ in equation 3, runs over all possible paths starting from a random point \mathbf{r}_0 and random end point. The first and second terms in equation 3 represent the contribution of molecules that photobleach and do not photobleach, respectively where

the $X_f(\mathbf{r}) = \eta(\mathbf{r})\Phi_f\sigma I(\mathbf{r})$ and $X_{bl}(\mathbf{r}) = \Phi_{bl}\sigma I(\mathbf{r})$. Here, $I(\mathbf{r})$ is the spatial dependence of intensity of the confocal laser beam (photons/area/time), $\eta(\mathbf{r})$ is the collection and detection efficiency of optics and electronics, Φ_f and Φ_{bl} are the fluorescence and photobleaching quantum yields, and σ is the absorption cross-section. Since the intensity of the excitation beam is low, no optical saturation effect was present. The all-silica nanochannels show negligible background and a steady background with respect to observation time [6]. So, I neglect the

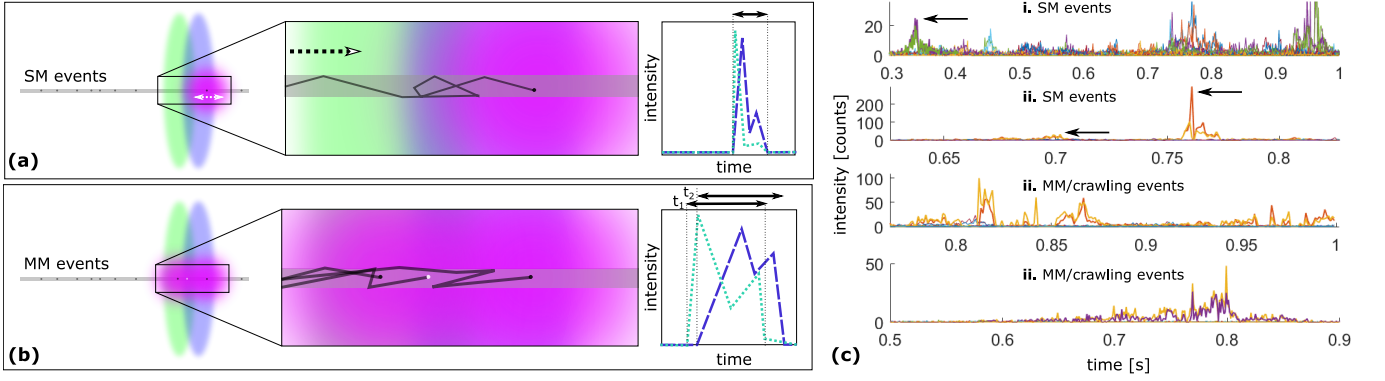


FIG. 1. **Single-molecule and multi-molecule events inside a channel that is narrower than the diffraction limit.** (a) The black dots represent photoactive single molecules, when they appear in the detection volume photon emission is represented with a blurry circle that is spatially larger than the diameter of the foci. (b) Multi-molecule (MM) events are situations when more than one photoactive molecule is present in a single focus or two foci, and they are emitting photons at the same time. Such signals are not easily distinguishable from molecules being dragged or crawling within the detection volume, which may result into photobleached/photo-inactive molecules – white dot represent them. (c) FEPI MC simulated 100 ms binned SM and MM events of 2 nm molecules. i. Short single-molecule bursts – two similar bursts at the same time refer to emission being detected by two detectors – the arrow represents such events. ii. Short single-molecule bursts with high intensity/photon numbers. iii. Reappearing bursts within millisecond timescale. iv. Long bursts suggest crawling of a single molecule.

background effects. The analytical expression of $P_1(N)$ is not possible; since the equation 3 runs over an infinite number of path, so it is fundamentally difficult to find a solution. Monte-Carlo sampling is done to calculate the $P_1(N)$ where random paths are chosen and remaining integration is performed numerically. A large number of random sampling over different paths leads to sufficiently precise approximation of $P_1(N)$.

Multi-molecule events i.e. close succession of more than one molecules flowing and leading to a single photon burst always have a nonzero probability. This will cause additional peaks with extra temporal broadening of the photon burst at higher burst size. I use a weighting factor w_k i.e. proportional to the probability that n molecules pass through the confocal volume, which are separated by less than the mean transit time leading to a single unresolved burst. Due to these n -molecule bursts, the BSD is the convolution of BSD for all $(n-1)$ -molecule bursts along with the BSD of pure single molecule burst. So, BSD for two-molecule is given by

$$P_2(N) = \sum_N P_1(N_1)P_1(N_2) \quad (4)$$

where $N = N_1 + N_2$, and BSD for $n > 2$ -molecule is given by

$$P_n(N) = \sum_{N_*} P_1(N_1)P_1(N_2)...P_1(N_n) \quad (5)$$

$$= \sum_N P_1(N_1)P_{n-1}(N_2)$$

where $N_* = N_1 + N_2 + ... + N_n$.

If τ_s is the minimum time between molecules leading to an unresolved prolonged burst, τ_m is the initial interval time during delivery of the molecules from the reservoir, w_n is proportional to the probability of n successive molecules, which are separated by less than τ_s time. No other molecules are present before and after this ‘molecular train’ within τ_s . In case of random arrival of the molecules, the probability density of τ before the arrival of the next molecule is $\tau_m^{-1} \exp(-\tau/\tau_m)$. For the probability of $\tau > \tau_s$ is $\exp(-\tau_s/\tau_m)$, which results to the weighting factor as

$$w_n = \exp\left(-\frac{\tau_s}{\tau_m}\right) \left[\prod_{j=1}^{n-1} \int_0^{\tau_s} \exp\left(-\frac{\tau_j}{\tau_m}\right) \frac{d\tau_j}{\tau_m} \right] \exp\left(-\frac{\tau_s}{\tau_m}\right) \quad (6)$$

$$= \exp\left(-\frac{2\tau_s}{\tau_m}\right) \left[1 - \exp\left(-\frac{\tau_s}{\tau_m}\right) \right]^{n-1}$$

Here, I consider a constant value of τ_s , which is modified in the algorithm with a thresholding loop. The initial condition of the numerical simulation was fed with spatial dependence of the intensity of the excitation laser $I(\mathbf{r})$, collection efficiency $\eta(\mathbf{r})$, and initial distribution of the molecule $p_0(\mathbf{r})$. The intensity distribution of a diffraction limited confocal laser beam is Gaussian. The nanochannels width and height are much smaller than the FWHM of the focus but the length is not (Figure 1). For the simplicity, I could neglect the Gaussian distribution in two axes for the quasi-1D nature of molecules’ presence inside nanochannel but I haven’t in the actual algorithm.

I have considered it as:

$$I(x, y) = \frac{2W}{\pi r_\omega^2} \exp \left[-2 \frac{x^2 - y^2}{r_\omega^2} \right] \quad (7)$$

$$\eta(x, y) = \frac{\eta_0}{\pi(1 - \cos \psi)} \times \left[\arcsin \frac{\sin \theta}{\cos \psi} - \cos \psi \arctan \left(\frac{\cos \psi \sin \theta}{\sqrt{\sin^2 \psi - \sin^2 \theta}} \right) \right]_{\theta_{\min}}^{\theta_{\max}} \quad (8)$$

where η_0 is the maximum value of the collection efficiency, $\psi = \arcsin(\text{NA}/n)$, $\theta_{\max} = \max(-\arctan((\frac{d}{2} - x)/|y|), -\psi)$ and $\theta_{\min} = \max(-\arctan((\frac{d}{2} - x)/|y|), -\psi)$, NA is the value of the numerical aperture, n is the refractive index, and d is the pinhole diameter in the object space. Here, $\theta_{\min} < \theta_{\max}$; if $\theta_{\min} > \theta_{\max}$, then $\eta(x, y)$ will be zero.

Employing a simple hydrodynamic model, I have calculated the distribution of the molecules at a position $x = x_0$ outside the slice of the confocal volume with diffraction limited focus. I have neglected the third dimension due to the nano-confinement. Although the molecules are confined within a diffraction limited space and only free to move in one direction, the multi-molecule events are still plausible since the molecules are smaller than the width and height of the nanochannels. Molecules are considered to be uniformly distributed over $x + c = y$; c is a spatial constant. From this starting plane, molecules accelerate to the laminar flow velocity and undergo a confined diffusion. The starting point $x = x_0$ of the Monte-Carlo simulation is considered at -3ω where the light intensity is negligible. Then, initial probability distribution p_0 is given by:

$$p_0(x, y) = \frac{x - x_0}{4\pi^2 y D \tau_0} \int_0^y d\mathbf{r} \int_0^{2\pi} d\phi \times \exp \left[-\frac{(y - \mathbf{r} \sin \phi)^2}{4D\tau_0} \right] \quad (9)$$

τ_0 is determined with respect to the pulsed frequency and the following equation:

$$\frac{x_0 - x_{\text{inj}}}{v_0} = \tau_0 - k^{-1}[1 - \exp(k\tau_0)] \quad (10)$$

k is an empirical flow acceleration constant.

III. SINGLE-MOLECULE AND MULTI-MOLECULE BURSTS IN CONFINED FLOW

The laminar flow profile is approximated to be negligible. However, further modelling suggests that I cannot neglect this despite the flow cross-sectional diameter is smaller than the confocal detection volume. The nanochannels are placed at the centre of the confocal volume. The diffusion coefficients of 2 nm and 20 nm size

where W denotes the power of the laser and r_ω is the waist radius. The spatial dependence (molecules are flowing along the x axis) of optical collection efficiency is given by:

molecules are 218 $\mu\text{m}^2/\text{s}$ and 21.8 $\mu\text{m}^2/\text{s}$, respectively. The time step used in the Monte-Carlo simulation was $\Delta\tau = 50 \mu\text{s}$, T was set to 3 ms, and the simulations sampled for 10^4 paths.

I use an experimental configuration as shown in Figure 1 where single molecules are flowing inside a nanochannel ($d_{nc} = 50 \text{ nm}$), and the nanochannel is placed inside two 640 nm foci are placed. The foci are shown in two different colours to emphasis they have orthogonal polarisation from each other – green and violet represent vertical and horizontal polarisation, respectively from the optical axis. They are spatially separated but slightly ($\approx 50 \text{ nm}$) overlapping two each other. A free flowing or diffusing single molecule passing by these two foci produces two bursts as schematically shown in Figure 1a with green and violet time trace signals. Ideally, single molecule bursts of a single species from two foci should have similar time duration and intensities. If a molecule interacts with the wall, which is highly likely when the mean free path is comparable to d_{nc} . Another possibility for longer time duration with higher intensity of bursts is in the case of multiple molecules being present in the foci with close successions as shown in Figure 1(b). Among these multimolecules there could be some photobleached molecules. In the simulation, I have considered an existence probability of a single molecule while undergoing photobleaching as mentioned in the theory section and supplementary Figure 1. A photobleached molecule also interacts with other molecules, and if it is adsorbed to the surface of the nanochannel then it is a constant source of interaction with the passing by molecules. Another instance that shows similar bursts characteristics with multi-molecule bursts is crawling of single molecules along the wall of nanochannels. In the FEPI MC simulations, I have tried to understand these multi-molecule events and single-molecule events. In Figure 1(c), I show FEPI MC simulated 100 ms binned single-molecule bursts of 2 nm sized molecules. The FEPI MC simulated bursts are hard to distinguish from an experimental data [6], which evidence the robustness of the algorithm. The arrow in the time-trace show some exemplary single molecule bursts. The first arrow in Figure 1(c)i represent a single-molecule bursts with minimal interaction in both the foci. In Figure 1(c)ii, I found a single-molecule burst with high intensity/photon numbers, which also shows a

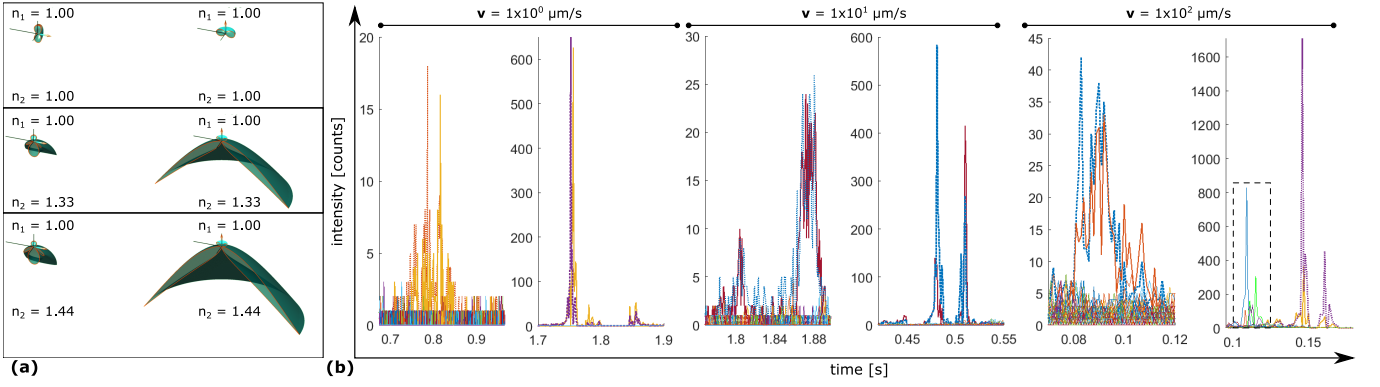


FIG. 2. **Electrodynamics of single-dipole and single-molecule bursts.** (a) Left figures – horizontal dipole and right figures – vertical (right) dipoles of λ_{640nm} are two ideal cases – electrodynamic interaction of single dipoles with heterogeneous interface strongly depends on refractive index mismatch; the electrical component of the emission pattern for dipoles creates are uniform doughnut shape for $n_1/n_2 = 1.00/1.00$ (top panel), $n_1/n_2 = 1.00/1.33$ has a larger distribution of electrical component towards n_2 for horizontal as well as vertical dipoles (mid panel), the trend continues for $n_1/n_2 = 1.00/1.44$ (bottom panel) – the emission intensity is larger for vertical dipole than horizontal dipole. (b) The FEPI MC simulation calculated single-molecule bursts of 20 nm molecule by considering the random orientation of single-dipole and its electrodynamic interactions at 1 $\mu\text{m/s}$, 10 $\mu\text{m/s}$, and 100 $\mu\text{m/s}$ flow velocities; characteristic burst sizes are ranging from less than 20 to 200 ms with low and high photon counts. Two signals at same time represent photons being emitted from two foci – non-identical bursts are due to two laser beams are orthogonally polarised to each other resulting to non-identical photon absorption by the single molecule.

crawling effect as shown by the first arrow. significantly long reappearing bursts within 250 ms is shown in Figure 1(c)iii, which seemed to be showing photo-inactive behaviour due to multi-molecule interactions. Another multi-molecule interactions for nearly 200 ms is shown in multi-molecule interactions.

To distinguish between crawling of single molecules on the nanochannel wall due to Knudsen type flow and multi-molecule interactions, we should investigate the electrodynamic interactions of single-molecule fluorescence with its surrounding, and later compare this with the temporal distributions. Figure 2a shows the electrodynamic interaction of single dipole with respect to orientation and refractive index mismatch of the interface. I plot the electrical field component at 640 nm wavelength for single horizontal and vertical dipoles' emission with respect to optical axis along of excitation. At a uniform interface with refractive indices $n_1/n_2 = 1.00/1.00$, uniform emission pattern is observed with a doughnut shape. Single-molecule experiments are often performed in water. Our single-molecule nanofluidic experiments were also taken place in water; $n_1/n_2 = 1.00/1.33$ represent an air-water interface where the dipole emission will have larger distribution of electrical component towards n_2 . For larger difference in refractive indices mismatch $n_1/n_2 = 1.00/1.44$, which is for air-silica/quartz interface as we used in the experiment. A noticeable difference is larger emission pattern for vertical dipole than horizontal dipole since absorption cross-section of a dipole is a function of its orientation/polarisability with respect to the field of excitation. The fluctuation in the bursts and its non-identical shapes in the Figure 1c and Figure 2b are justified considering the stochastic electrodynamic interactions due to the randomness of confined

interactions inside the nanofluidic channels. In Figure 2c, we have shown the bursts for different flow velocities ranging from 1 $\mu\text{m/s}$ to 100 $\mu\text{m/s}$ of 20 nm sized fluorophores. The two foci are orthogonally polarised from each other. Hence, differences in fluorescence intensities of single molecule bursts are not unexpected. In some cases, we see clearly anti-correlated intensities, for example, the high intensity bursts of 1 $\mu\text{m/s}$ and 10 $\mu\text{m/s}$. The single-molecule bursts inside the box of 100 $\mu\text{m/s}$ is highly anti-correlated.

IV. TEMPORAL DISTRIBUTION OF BURSTS

The temporal burst size distribution of non-interacting single molecules should be a δ -function. The FEPI MC considers a δ -function functional considering the complex interactions of single-molecule fluorescence experiments inside the nanofluidic channel as shown in the equation 3. The histogram of temporal response of single-molecule bursts will show the statistical nature of the complex interactions. As shown in Figure 3a, a histogram of single-molecule burst size (defined with time unit) for 20 nm sized single molecules paths through focus 1 and 2 different velocities ranging from 0.01 $\mu\text{m/s}$ to 10 $\mu\text{m/s}$. Here, I overlap the histograms of 1000 path through focus 1 (blue) and focus 2 (red). All the histograms have a broad time distribution of approximately 400 ms. If we look carefully, at slower velocities for example at 0.01 $\mu\text{m/s}$ and 0.1 $\mu\text{m/s}$, we can find discreet peaks within the broad time distribution. These are due to favourable interactions, which can be temporal signatures of nanoconfined photophysical interactions of single molecules. Among them at this time range 210 ms to 230 ms single-molecule

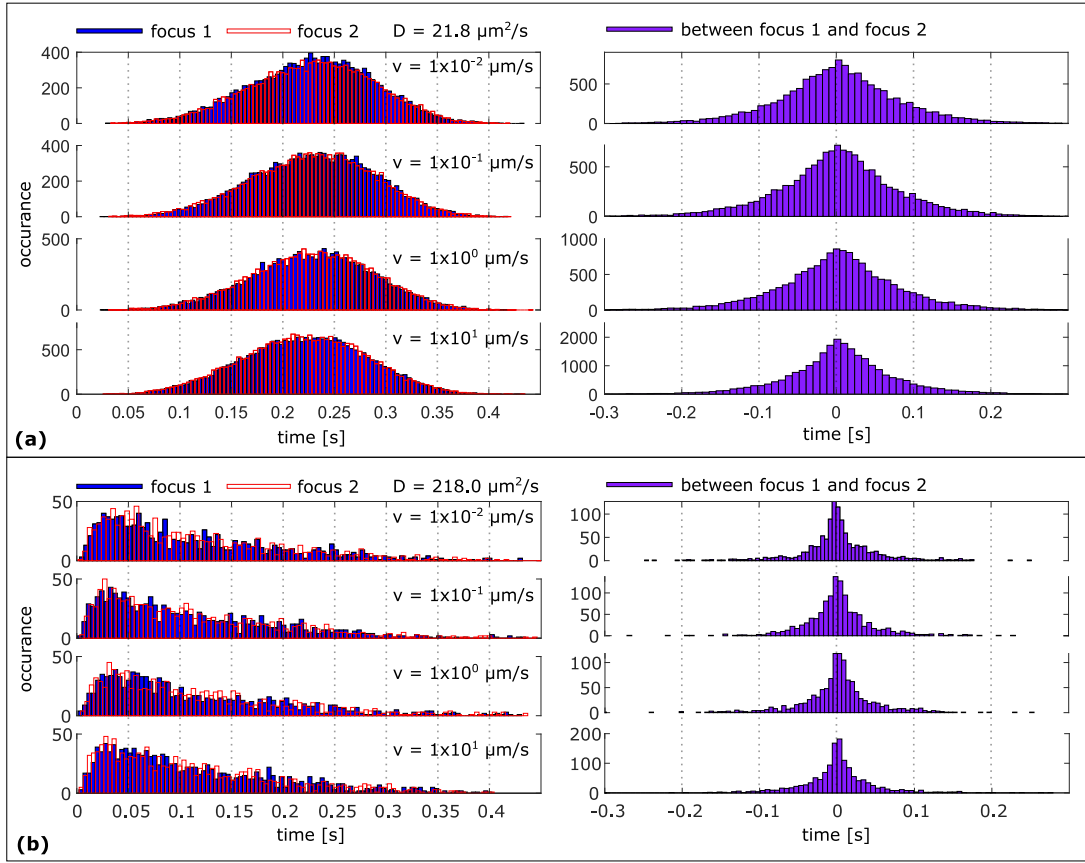


FIG. 3. Single-molecule burst size distribution. (a) LHS: Histogram of 1000 paths in focus 1 and 2 for 20 nm sized single molecules flowing at the velocities $0.01 \mu\text{m/s}$ (230 ms with highest occurrence), $0.1 \mu\text{m/s}$ (220 ms with highest occurrence), $1 \mu\text{m/s}$ (210 ms with highest occurrence), and $10 \mu\text{m/s}$. Multiple peaks are present in $0.01 \mu\text{m/s}$ and $0.1 \mu\text{m/s}$, a flattening feature (200 to 250 ms with highest occurrence) appears due to the flow velocity contribution in $1 \mu\text{m/s}$ and $10 \mu\text{m/s}$. RHS: Histogram of time distribution between focus 1 and focus 2, the spread narrows down from top to bottom due to increasing flow velocity. Molecular interactions are visible in $0.01 \mu\text{m/s}$ to $1 \mu\text{m/s}$ in positive and negative sides. (b) LHS: Burst size distribution in focus 1 and 2 of 2 nm single molecules flowing at velocities $0.01 \mu\text{m/s}$, $0.1 \mu\text{m/s}$, $1 \mu\text{m/s}$, and $10 \mu\text{m/s}$ – highest occurrence within 50 ms. The short timescale bursts from 0 to 60 ms are due to single molecule transitions. Larger burst sizes up to 400 ms are due to strong interactions with the nanofluidic environment. At $1 \mu\text{m/s}$ and $10 \mu\text{m/s}$, the single molecule bursts and other interactions are smeared together cannot be distinguished separately. RHS: Time distribution of molecules between focus 1 and focus 2 – narrower distribution at $10 \mu\text{m/s}$ compare to low flow velocities.

bursts are most frequently occurring, such as 230 ms for $0.01 \mu\text{m/s}$ has, 220 ms for $0.1 \mu\text{m/s}$, 210 ms for $1 \mu\text{m/s}$, and 200 ms to 250 ms for $10 \mu\text{m/s}$. At $10 \mu\text{m/s}$, a 50 ms flat peak is observed, which suggests equal probability of several kinds of interaction. Since we have two sources of signal for a single molecule, let us mathematically compare the time distribution between focus 1 and focus 2. The spread between two foci reduces from 400 ms to 200 ms with increasing velocities as shown in the right panel of Figure 3a.

A contrasting difference is observed in the burst size distribution if we reduce an order of magnitude in the size of the single molecule. For 2 nm size, the peak the histogram shifts to faster timescale of 25 – 50 ms and shape of the histogram is positive skewed as shown in Figure 3b. The histogram for $0.01 \mu\text{m/s}$ shows high occurrences at fast timescale 25 ms, 60 ms, and 80 ms along with sev-

eral low occurrences of long bursts at slow timescale up to 400 ms. The distribution at faster timescale are for single-molecule bursts, which had less interactions and passed through the foci with short intervals. Specifically, the sub-25 ms timescale bursts are non-interacting single-molecule crossings, and the 50 to 100 ms timescale bursts are responsible for molecular shot noise i.e. molecular interactions among multiple single molecules. Molecular shot noise are temporary events when molecule to molecule interacts, such events can be spectrally resolved by studying the shift in emission peak as well as with phononic spectroscopy if high SNR is available. The slower occurrences are due to single-molecule interactions with the walls, earlier we referred them as crawling events of single molecule or multi-molecules. At slow velocities, the single-molecule crossings, molecular shot-noise, and crawling events can be well identified, which get smeared

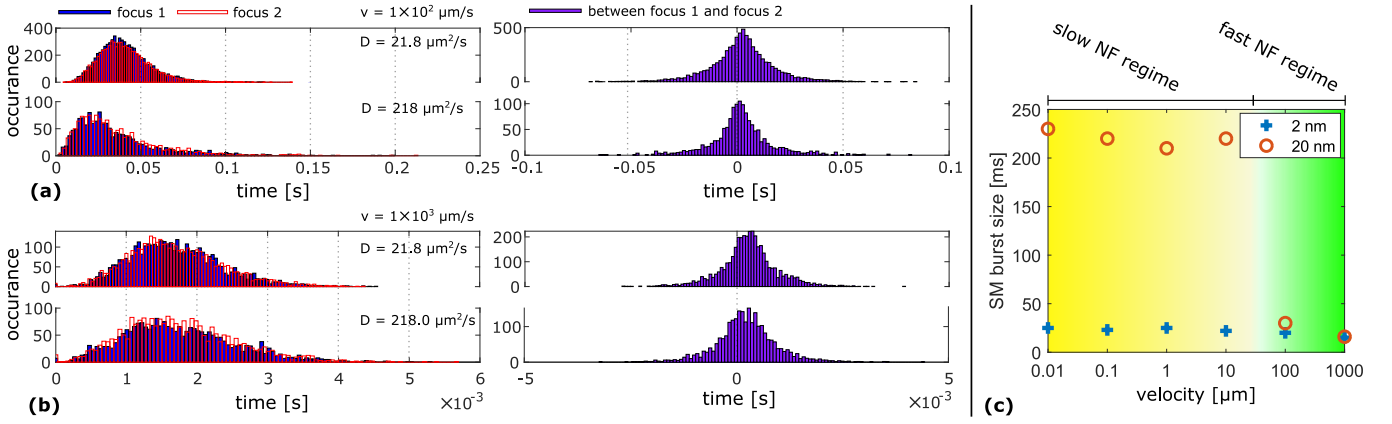


FIG. 4. **Burst size distribution of fast nanofluidics regime.** (a) At flow velocity $100 \mu\text{m/s}$, 20 nm ($D = 21.8 \mu\text{m}^2/\text{s}$) has highest occurrence of 33 ms bursts and 2 nm ($D = 21.8 \mu\text{m}^2/\text{s}$) with 20 ms with a global Poissonian distribution. (b) At $1000 \mu\text{m/s}$ flow velocity, 20 nm molecule shows highest occurrence at 1.5 ms , and 2 nm molecule has flat distribution of high occurrence from 1 to 2 ms . (c) Single-molecule nanofluidic regimes – in FEMC simulation, the effect of nanofluidic regimes on single-molecule bursts of 20 nm single molecules is considerably visible compare to 2 nm single molecules.

away at fast velocities as shown in Figure 3b. The time distribution between focus 1 and focus 2 is narrower at $10 \mu\text{m/s}$ compare to slow flow velocities as shown in the right panel of Figure 3b. The time distributions also show fine temporal following the analysis timescale of different single-molecule bursts characteristics.

From the findings shown in Figure 3, I classify the flow velocities ranging from $0.01 \mu\text{m/s}$ to $10 \mu\text{m/s}$ as ‘slow nanofluidic regime’ because the diffusion behaviour and strong interactions of confinement effect are dominating characteristic feature of this regime. Irrespective of the order of magnitude differences in flow velocities, we can identify reproducible slow nanofluidic regime characteristics. Following the scaling law, the 20 nm molecules show single-molecule bursts at around 220 ms while sub- 25 ms timescale events are for 2 nm single molecule bursts. The broad spread of occurrence in 20 nm single molecules at this nanofluidic regime show strong interactions/crawling effect and molecular shot noise.

Unlike the slow nanofluidic regime, the characteristics of histogram from $100 \mu\text{m/s}$ is so different from one flow velocity to another that I use different timescales to show the details of their histograms. Thus, I define ‘fast nanofluidic regime’ from $100 \mu\text{m/s}$ velocity as shown in Figure 4. Figure 4a shows histograms of 20 nm and 2 nm single molecules at $100 \mu\text{m/s}$ with highest occurrence at 33 ms and 20 ms , respectively. At this flow regime, the aforementioned interactions of single molecules are not strong, specifically for the 20 nm molecules. The molecular shot noise and crawling events are limited. However, for the 2 nm molecules, the molecular shot noise scales down to faster time scale as we can see a distribution of this peak at 38 ms along with a small contribution due to crawling events. It is noticeable that the sub- 20 ms bursts for 2 nm molecules is consistent at fast nanofluidic regime. The time distributions between two foci also suggest the same in the right panel. The trend continues to

$1000 \mu\text{m/s}$ in Figure 4b. At this flow velocity, it is hard to distinguish between the histograms of 20 nm and 2 nm single molecules, except the fine features. At the fast nanofluidic regime, the driving force for flow large enough to overcome the crawling events. For an overall understanding, Figure 4c shows single-molecule burst sizes of the two identified nanofluidic regimes with respect to the flow velocities.

V. SUMMARY

The Feynman-Enderlein path integral is a powerful method to model the complex single-molecule nanofluidics and show two distinct single-molecule nanofluidic regimes. I have showed how to resolve the complexity of single-molecule nanofluidics by integrating electrodynamics. In future, the method will be integrated with the electrostatic effects to deal with the Debye-length related issues. The FEMC method has not been used widely in the single-molecule experiments. This method opens up several avenues in biophysics as well as quantum hydrodynamics. Single fluorophores to misfolded proteins, nanobodies, and quantum dots in solid state nanochannels/tunnelling nanotubes or within lipid bilayers are all relevant for this work.

VI. ACKNOWLEDGEMENT

The research was funded by the German Research Foundation/Deutsche Forschungsgemeinschaft (DFG) – Project number 405479535 (DFG Research Fellowship – PI Siddharth Ghosh). I am most thankful to Professor Joerg Enderlein for many important discussions during 2012-2016 from where this work is initiated and for laying the foundation of this work. I am also thankful to

Professor Jeremy Baumberg’s comments during the S3IC 2020 Conference in Munich and later encouragement to work in this field. The work utilised computational resources provided by Professor Tuomas Knowles at the

Maxwell Centre and Yusuf Hamied Department of Chemistry, University of Cambridge. My sincere gratitude to Professor Allard Mosk for his valuable comments in the manuscript.

-
- [1] H. P. Lu, L. Xun, and X. S. Xie, *Science* **282**, 1877 (1998).
 - [2] A. E. Cohen and W. Moerner, *Proceedings of the National Academy of Sciences* **103**, 4362 (2006).
 - [3] P. Zijlstra, P. M. Paulo, and M. Orrit, *Nature nanotechnology* **7**, 379 (2012).
 - [4] M. D. Baaske, M. R. Foreman, and F. Vollmer, *Nature nanotechnology* **9**, 933 (2014).
 - [5] J. F. Lesoine, P. A. Venkataraman, P. C. Maloney, M. E. Dumont, and L. Novotny, *Nano letters* **12**, 3273 (2012).
 - [6] S. Ghosh, N. Karedla, and I. Gregor, *Lab on a Chip* **20**, 3249 (2020).
 - [7] E. M. Purcell, in *Confined Electrons and Photons* (Springer, 1995) pp. 839–839.
 - [8] J. Enderlein, *Biophysical Journal* **78**, 2151 (2000).
 - [9] N. Karedla, S. C. Stein, D. Hähnel, I. Gregor, A. Chizhik, and J. Enderlein, *Physical review letters* **115**, 173002 (2015).
 - [10] F. Westerlund, F. Persson, A. Kristensen, and J. O. Tegenfeldt, *Lab on a Chip* **10**, 2049 (2010).
 - [11] C. Eggeling, S. Berger, L. Brand, J. Fries, J. Schaffer, A. Volkmer, and C. Seidel, *Journal of biotechnology* **86**, 163 (2001).
 - [12] M. Orrit, *Colloids and Surfaces B: Biointerfaces* **74**, 396 (2009).
 - [13] P. v. Debye and E. H.ückel, *phys. Z* **24**, 185 (1923).
 - [14] R. H. French, V. A. Parsegian, R. Podgornik, R. F. Rafter, A. Jagota, J. Luo, D. Asthagiri, M. K. Chaudhury, Y.-m. Chiang, S. Granick, *et al.*, *Reviews of Modern Physics* **82**, 1900 (2010).
 - [15] J. Enderlein, D. L. Robbins, W. P. Ambrose, and R. A. Keller, *The Journal of Physical Chemistry A* **102**, 6089 (1998).
 - [16] K. Malek and M.-O. Coppens, *The Journal of chemical physics* **119**, 2801 (2003).
 - [17] S. Li, Y. Wang, K. Zhang, and C. Qiao, *Industrial & Engineering Chemistry Research* **58**, 21772 (2019).
 - [18] R. P. Feynman, *California Institute of Technology, Engineering and Science magazine* (1960).
 - [19] E. Schrodinger, *What is life?: With mind and matter and autobiographical sketches* (Cambridge University Press, 2012).
 - [20] M. Loose, E. Fischer-Friedrich, J. Ries, K. Kruse, and P. Schuille, *Science* **320**, 789 (2008).
 - [21] T. Litschel, K. A. Ganzinger, T. Movinkel, M. Heymann, T. Robinson, H. Mutschler, and P. Schuille, *New Journal of Physics* **20**, 055008 (2018).
 - [22] R. Golestanian, *Physical review letters* **115**, 108102 (2015).
 - [23] P. Illien, X. Zhao, K. K. Dey, P. J. Butler, A. Sen, and R. Golestanian, *Nano letters* **17**, 4415 (2017).
 - [24] M. Ghosh, S. Ghosh, M. Seibt, K. Y. Rao, P. Peretzki, and G. M. Rao, *CrystEngComm* **18**, 622 (2016).
 - [25] M. Ghosh, S. Ghosh, H. Attariani, K. Momeni, M. Seibt, and G. Mohan Rao, *Nano letters* **16**, 5969 (2016).
 - [26] J. Enderlein, *Single Molecules* **1**, 225 (2000).
 - [27] A. E. Cohen, *Trapping and manipulating single molecules in solution*, Ph.D. thesis, Stanford University (2007).
 - [28] J. Ranzinger, A. Rustom, M. Abel, J. Leyh, L. Kihm, M. Witkowski, P. Scheurich, M. Zeier, and V. Schwenger, *PLoS One* **6**, e29537 (2011).
 - [29] J. Jeffet, A. Kobo, T. Su, A. Grunwald, O. Green, A. N. Nilsson, E. Eisenberg, T. Ambjornsson, F. Westerlund, E. Weinhold, *et al.*, *ACS nano* **10**, 9823 (2016).
 - [30] Z. Ristanovic, A. D. Chowdhury, R. Y. Brogaard, K. Houben, M. Baldus, J. Hofkens, M. B. Roeflaers, and B. M. Weckhuysen, *Journal of the American Chemical Society* **140**, 14195 (2018).
 - [31] J. K. Holt, H. G. Park, Y. Wang, M. Stadermann, A. B. Artyukhin, C. P. Grigoropoulos, A. Noy, and O. Bakajin, *Science* **312**, 1034 (2006).
 - [32] R. H. Tunuguntla, R. Y. Henley, Y.-C. Yao, T. A. Pham, M. Wanunu, and A. Noy, *Science* **357**, 792 (2017).
 - [33] T. Basché, W. Moerner, M. Orrit, and H. Talon, *Physical review letters* **69**, 1516 (1992).
 - [34] S. Ghosh, A. M. Chizhik, N. Karedla, M. O. Dekaliuk, I. Gregor, H. Schuhmann, M. Seibt, K. Bodensiek, I. A. Schaap, O. Schulz, *et al.*, *Nano letters* **14**, 5656 (2014).
 - [35] R. A. Keller, W. P. Ambrose, P. M. Goodwin, J. H. Jett, J. C. Martin, and M. Wu, *Applied Spectroscopy* **50**, 12A (1996).
 - [36] J. P. Torella, S. J. Holden, Y. Santoso, J. Hohlbein, and A. N. Kapanidis, *Biophysical journal* **100**, 1568 (2011).
 - [37] D. Chen and N. J. Dovichi, *Analytical Chemistry* **68**, 690 (1996).
 - [38] T. Dertinger, V. Pacheco, I. von der Hocht, R. Hartmann, I. Gregor, and J. Enderlein, *ChemPhysChem* **8**, 433 (2007).
 - [39] S. Chiantia, J. Ries, N. Kahya, and P. Schuille, *ChemPhysChem* **7**, 2409 (2006).
 - [40] P. S. Dittrich and P. Schuille, *Analytical chemistry* **74**, 4472 (2002).
 - [41] G. U. Nienhaus, P. Maffre, and K. Nienhaus, in *Methods in enzymology*, Vol. 519 (Elsevier, 2013) pp. 115–137.
 - [42] R. P. Feynman and L. M. Brown, *Feynman’s thesis: a new approach to quantum theory* (World Scientific, 2005).
 - [43] J. Enderlein, D. L. Robbins, W. P. Ambrose, P. M. Goodwin, and R. A. Keller, *Bioimaging* **5**, 88 (1997).